Optics Letters

Unidirectional waveguide grating antennas with uniform emission for optical phased arrays

Manan Raval,*,† Christopher V. Poulton,† and Michael R. Watts

Research Laboratory of Electronics, Massachusetts Institute of Technology, Cambridge, Massachusetts 02139, USA
**Corresponding author: mraval@mit.edu*

Received 26 April 2017; accepted 29 May 2017; posted 6 June 2017 (Doc. ID 294606); published 28 June 2017

We demonstrate millimeter-scale optical waveguide grating antennas with unidirectional emission for integrated optical phased arrays. Unidirectional emission eliminates the fundamental problem of blind spots in the element factor of a phased array caused by reflections of antenna radiation within the substrate. Over 90% directionality is demonstrated using a design consisting of two silicon nitride layers. Furthermore, the perturbation strength along the antenna is apodized to achieve uniform emission for the first time, to the best of our knowledge, on a millimeter scale. This allows for a high effective aperture and receiving efficiency. The emission profile of the measured 3 mm long antenna has a standard deviation of 8.65% of the mean. These antennas are state of the art and will allow for integrated optical phased arrays with blind-spot-free high transmission output power and high receiving efficiency for LIDAR and free-space communication systems.

OCIS codes: (130.3120) Integrated optics devices; (110.5100) Phased-array imaging systems.

https://doi.org/10.1364/OL.42.002563

Silicon photonic phased arrays for light detection and ranging (LIDAR) and free-space communication applications [1–9] have garnered a great deal of interest in recent years, given the advancements in CMOS foundry processes for large-scale silicon photonic integration. Practical implementations of integrated optical phased arrays for both applications require large optical apertures to maintain a small diffraction angle and provide a large receiving area. In one-dimensional arrays, long waveguide grating antennas (WGAs), formed by patterning periodic perturbations in an integrated waveguide, have been widely explored for achieving large apertures since their length may be scaled to several millimeters [3,4]. WGAs demonstrated to date have near-equal radiation in the upward and downward directions due to designs that do not have sufficient vertical asymmetry. Any downward antenna radiation undergoes multiple reflections in the silicon handle wafer and gives rise to a set of interference fringes in the element factor [10] of the antenna. This phenomenon decreases the output power of a phased array by over 70% when steering a beam through points of destructive interference, resulting in blind spots in the field of view (FOV).

Additionally, WGAs employed in demonstrations of large-scale phased arrays have primarily been designed with uniform perturbation strength along the antenna length [1,3,4]. This produces an exponentially decaying emission profile in the antenna dimension, thereby reducing the effective aperture of the phased array for a given chip footprint. For receivers, the effective aperture determines the on-chip collection area; for transmitters, a large effective aperture provides a small diffraction angle for long-range applications. Therefore, employing WGAs with uniform perturbation strength can limit system capabilities, including receiver efficiency and practical propagation range.

In this Letter, a millimeter-scale unidirectional silicon nitride WGA with uniform emission is demonstrated. The antenna is implemented in a dual-layer silicon nitride waveguide. Unidirectional emission is achieved by patterning identical periodic inward perturbations in the two layers that are spatially offset in the direction of propagation. While offset perturbations have been shown for achieving unidirectional fiber grating couplers [11–14], to the best of our knowledge, this Letter is the first demonstration of millimeter-scale unidirectional WGAs that may be densely arrayed for realizing large-aperture phased arrays similar to [4]. A 3 mm long WGA designed to exhibit over 93% upward emission is presented with significant suppression of fringes in the element factor caused by reflections within the substrate. Furthermore, the perturbation strength is apodized along the length of the antenna to generate a uniform emission profile for increasing the effective aperture, compared to that provided by an exponential profile [6,15]. The standard deviation of the measured emission intensity of the presented antenna was 8.65% of the mean.

A ray-optic schematic representation of the emission of an optical antenna in a silicon photonic chip is shown in Fig. 1(a). Downward radiation experiences multiple reflections in the substrate before eventually being emitted upward. This creates a Fabry–Perot cavity with a transmission response that varies with angle. The effect of this cavity on the element factor may be understood by considering the behavior of a source with isotropic radiation for small ranges of angles around $\theta = 0°$ (upward direction) and $\theta = 180°$ (downward direction), with θ as defined in Fig. 1(a). In this model, the ratio of the amplitudes of the isotropic radiation in the upward and downward directions is set to equal $\frac{d}{(1-d)}$, where d is

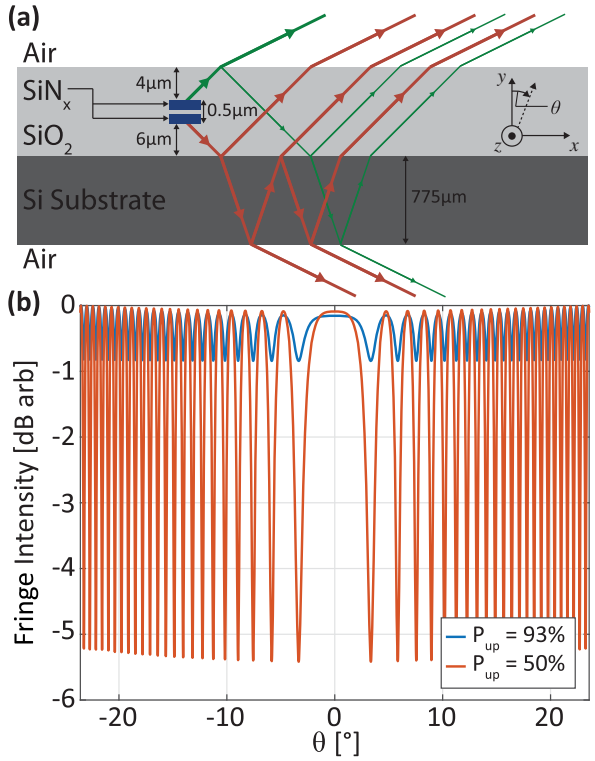

Fig. 1. (a) Schematic of multiple reflections in the silicon substrate and overlying photonic layer stack. The green and red lines represent the optical pathways of the upward and downward radiation, respectively, of the antenna. (b) Fringe patterns in the element factor with 50% and 93% upward directionality.

directionality defined as the percentage of total power radiated upward. If a source with $d = 50\%$ is placed in the material stack-up used in this Letter [Fig. 1(a)], the interference fringes shown in Fig. 1(b) appear in the element factor [10]. This decreases the transmitted or received power of a phased array by up to 5.3 dB at locations of maximum destructive interference. This interference is especially detrimental to transmit/receive (TX/RX) phased array systems, in which a total signal-to-noise ratio (SNR) reduction of 10.6 dB would be observed at certain locations in the FOV. As shown in Fig. 1(b), power loss at blind spot locations is reduced to 0.69 dB with 93% upward directionality, corresponding to only a 1.38 dB SNR decrease in TX/RX systems.

In order to reduce the element factor fringes, a unidirectional WGA was designed in a silicon nitride material platform. Silicon nitride is beneficial for high-power, large-aperture optical phased arrays due to the low nonlinearities [4]. Furthermore, utilizing low-index contrast waveguides easily allows for WGAs with weak perturbations formed by directly etching the waveguide without the need for a very accurate shallow etch. It is also straightforward to have multiple layers of silicon nitride [16,17] to break vertical symmetry and realize unidirectionality, whereas having multiple layers of crystalline silicon is a significant challenge [18]. Here, two 200 nm thick silicon nitride layers with a separation gap of 100 nm were used, as shown in Fig. 2(a). The antenna is formed by patterning periodic full-etch inward perturbations in a 1.0 μm wide waveguide. These perturbations are identical in the two waveguide layers, but spatially offset in the direction of propagation by length L_o. A unidirectional emitter can be realized with two scattering elements with a $\lambda/4$ displacement, both vertically and horizontally, to produce constructive interference in one vertical direction and destructive in the other [19]. Here, the fixed silicon nitride layer thicknesses and separation gap prevent complete constructive interference in the upward emission. Therefore, unidirectionality is achieved by determining the offset length L_o which yields maximum destructive interference in the downward emission.

In order to design the WGA, each period of the grating may be decomposed into four distinct regions, I-IV, with different waveguide cross sections and associated effective indices, as illustrated in Fig. 2(a). The effective index n_{full} of the full-width waveguide region remains constant, while the effective indices n_s and n_a of symmetric and asymmetric perturbed waveguide regions, respectively, change with perturbation value p. Indices n_s and n_a may be calculated using an eigenmode solver and are plotted in Fig. 2(b). The WGA presented here is designed to emit directly upward at the design wavelength of 1550 nm. Therefore, the lengths of the four waveguide regions must be chosen such that the total optical path length of a single period is equal to one wavelength as follows:

$$\lambda_0 \equiv \underbrace{(L_f - L_o)n_{\text{full}}}_{\text{Region I}} + \underbrace{(L_p(p) - L_o)n_s(p)}_{\text{Region III}} + \underbrace{2L_o n_a(p)}_{\text{Regions II/IV}}, \quad (1)$$

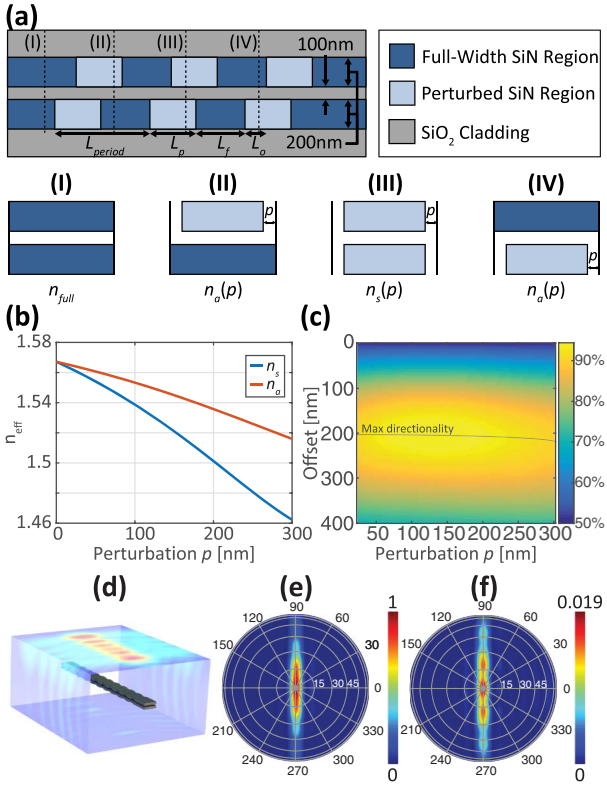

Fig. 2. (a) Side-view (yz-plane) cross section of the unidirectional WGA and transverse (xy-plane) cross sections of regions I-IV of a grating period. (b) Simulated effective indices n_a and n_s. (c) Simulated directionality. (d) FDTD simulation of radiation from a WGA with $p = 100$ nm and the corresponding far fields of the (e) upward and (f) downward emission.

where λ_0 is the design wavelength, L_f and L_p are the lengths of the full-width and perturbed regions, respectively, in a single waveguide layer, and L_o is the length of the spatial offset between the two layers. When designing the antenna, either L_f or L_p can be fixed, while p and other length parameters are changed to obtain the desired perturbation strength and optimize unidirectionality. Here, L_f is fixed to 500 nm. Then, for a particular value of p, the offset L_o is swept across a range of values in a finite-difference time-domain (FDTD) simulation of a short section of the antenna composed of 10 periods to determine the resulting directionality. For each point in the sweep, the length L_p is set to maintain the condition in Eq. (1) and can be determined by rewriting Eq. (1) as

$$L_p(p) = \frac{\lambda_0 + L_o(n_{\text{full}} + n_s(p) - 2n_a(p)) - L_f n_{\text{full}}}{n_s(p)}. \quad (2)$$

Figure 2(c) shows the simulated antenna directionality for a range of values for p and L_o. It can be seen that the L_o yielding maximum upward directionality (thus, also L_p) changes slightly as p is increased. Figure 2(d) shows the radiated electric field amplitude calculated using FDTD for the optimized antenna at $p = 100$ nm when no silicon substrate is included. The corresponding far-field radiation profiles of the upward and downward emission [Figs. 2(e)–2(f)] show over an order of magnitude lower peak power in the downward emission.

The simulation data in Fig. 2(c) demonstrate that high upward directionality is achieved for a wide range of perturbations. This enables arbitrary apodization of the antenna emission rate, while maintaining a low extinction ratio of fringes in the element factor. A WGA with constant perturbations will emit an exponential profile that follows $e^{-\beta z}$, where β is the perturbation strength and z is the direction of propagation along the antenna. β is determined by the perturbation value p of the antenna. For a given perturbation value, β may be approximated from the previously described FDTD simulation as $\beta(p) = (1 - T(p))/(10 \times (L_f + L_p(p)))$, where T is the light remaining in the waveguide after 10 periods for an antenna with optimized L_o. Figure 3(a) shows the perturbation strength as a function of perturbation value, along with the grating period needed to maintain Eq. (1). By changing the perturbation value, β can be altered by over two orders of magnitude.

In order to realize uniform emission throughout the antenna, the required perturbation strength profile can be calculated with the differential equation

$$\frac{dW(z)}{dz} = -\beta(z)W(z) = -S(z), \quad (3)$$

where $W(z)$ is the power of the guided light in the antenna at location z, $\beta(z)$ is the perturbation strength at location z, and $S(z)$ is the power of the light scattered at location z. The beginning of the antenna is defined to be at $x = 0$, and the total physical length of the antenna is defined as L_0. If $S(z)$ is set to be uniform, $S(z) \equiv 1/L$; then $\beta(z)$ is solved to be a hyperbolic function $\beta(z) = \frac{1}{L-z}$, where L is some constant such that $L \geq L_0$ for $\beta(z)$ to remain positive. For uniform emission, it is not necessary for L to equal L_0, in which case there is some non-emitted light at the end of the antenna. This allows for tailoring the required perturbation strength profile, if a strong perturbation cannot be achieved in a given material platform. It can also be beneficial to make the perturbation strength not have a sharp change at the end of the antenna. However, if $L \neq L_0$, the percentage of power that is emitted is $\int_0^{L_0} S(z)dz = L_0/L$. A 3 mm long ($L_0 = 3$ mm) unidirectional WGA with a uniform emission profile was designed with $L = 3.05$ mm using the simulated data in Fig. 3(a) and its parameters as a function of z are plotted in Fig. 3(b).

WGAs presented in this Letter were fabricated on a 300 mm wafer with 6 μm buried oxide (BOX) in a commercial CMOS foundry. Both 200 nm thick silicon nitride layers were deposited using a plasma-enhanced chemical vapor deposition process and patterned using 193 nm immersion lithography. The near and far fields of these WGAs were characterized using an imaging setup similar to that shown in [1]. The measured element factor of a 3 mm long single-silicon-nitride-layer antenna designed with uniform emission is shown in Fig. 4(a). This antenna is vertically symmetric and, therefore, exhibits bidirectional radiation in the upward and downward directions. As expected, significant intensity variations appear in the element factor of the bidirectional antenna due to reflections within the substrate. In contrast, the unidirectional antenna with the same length exhibits a much more uniform element factor [Fig. 4(b)] with intensity variations remaining below 1.56 dB. Additionally, a unidirectional WGA variant, with identical design parameters but flipped in the vertical dimension, was also fabricated. This antenna directs radiation downward into the substrate, resulting in an element factor that is dominated by interference fringes due to reflections in the silicon handle wafer, as seen in Fig. 4(c).

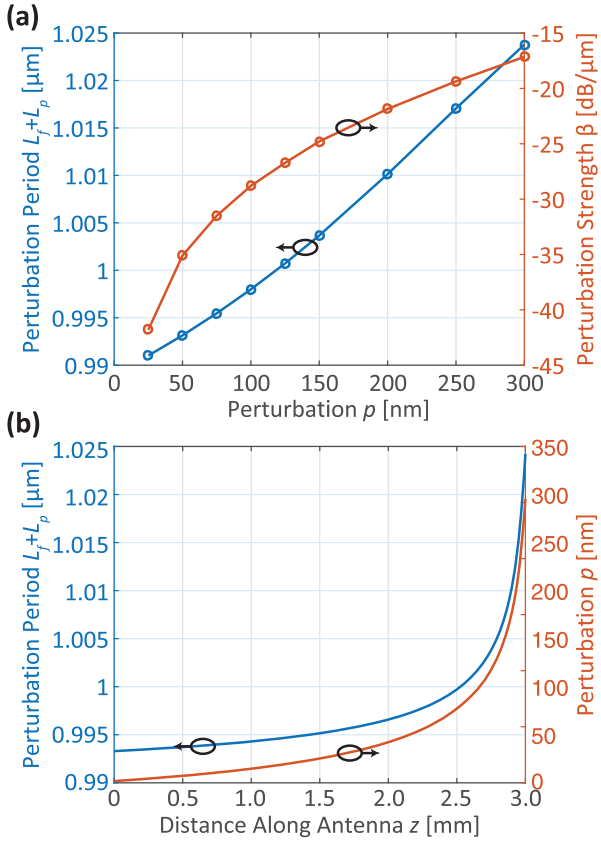

Fig. 3. (a) Simulated perturbation strength and corresponding WGA period of each p with optimized unidirectionality. (b) Synthesized apodized antenna parameters for a $L_0 = 3$ mm antenna with $L = 3.05$ mm.

An image of the near field of the above unidirectional antenna is shown in Fig. 4(d). For comparison, a near-field image of a unidirectional WGA with a constant perturbation of $p = 82$ nm is shown in Fig. 4(e). This value of p yields a WGA with emission that exponentially decays to e^{-2} at $z = 3$ mm. Plots of the emission intensity along the length of the antenna with both constant and apodized perturbation strengths are shown in Fig. 4(f). The results from the constant β antenna show the accuracy between the simulated and expected value of β. This accuracy allows for the uniform emission antenna to work as designed and more efficiently utilize the antenna aperture. For the antenna with perturbation strength apodization shown here, the standard deviation of the radiation intensity is 8.65% of the mean.

In conclusion, we have presented the design and experiment of silicon nitride unidirectional WGAs with perturbation strength apodization for uniform emission. To the best of our knowledge, this is the first demonstration of millimeter-scale unidirectional WGAs that may be densely arrayed for constructing high-power large-aperture phased arrays for applications including LIDAR and free-space optical communications. Unidirectional emission suppresses the extinction ratio of interference fringes that appear in the element factor of optical antennas due to reflections within the silicon substrate. This mitigates the fundamental problem of decreased transmitted and received power at locations of destructive interference. 3 mm long WGAs with over 93% simulated upward directionality were demonstrated. The extinction ratio of interference fringes in the element factor was experimentally reduced to lower than 1.56 dB in these antennas. Additionally, the perturbation strength was varied along the length of the antenna to achieve uniform emission in the near field. As compared to a phased array with an exponentially decaying emission profile, one with a uniform near field provides a larger effective aperture and allows for a higher mode overlap with received plane waves. Finally, while devices demonstrated in this Letter were 3 mm long, the antenna synthesis process detailed in this report may be used to arbitrarily scale the length of the presented unidirectional uniform emission WGA design in the future.

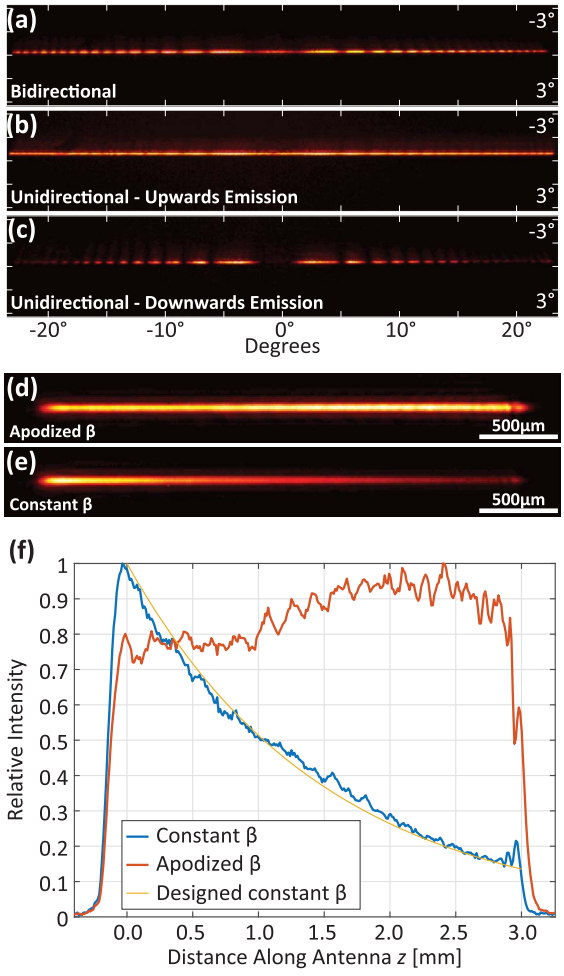

Fig. 4. Measured element factors of (a) a bidirectional WGA and (b), (c) unidirectional WGAs fabricated with upward and downward emission. (d),(e) IR camera images of near-field radiation of WGAs with constant and apodized perturbation strength with (f) corresponding plots.

Funding. Defense Advanced Research Projects Agency (DARPA) E-PHI program (HR0011-12-2-0007).

Acknowledgment. The authors thank Dr. Joshua Conway for helpful discussions and Patrick Callahan for coordinating the top-level mask assembly.

†These authors contributed equally to this Letter.

REFERENCES

1. J. Hulme, J. Doylend, M. Heck, J. Peters, M. Davenport, J. Bovington, L. Coldren, and J. Bowers, Opt. Express **23**, 5861 (2015).
2. H. Abediasl and H. Hashemi, Opt. Express **23**, 6509 (2015).
3. D. N. Hutchison, J. Sun, J. K. Doylend, R. Kumar, J. Heck, W. Kim, C. T. Phare, A. Feshali, and H. Rong, Optica **3**, 887 (2016).
4. C. V. Poulton, M. J. Byrd, M. Raval, Z. Su, N. Li, E. Timurdogan, D. Coolbaugh, D. Vermeulen, and M. R. Watts, Opt. Lett. **42**, 21 (2017).
5. F. Aflatouni, B. Abiri, A. Rekhi, and A. Hajimiri, Opt. Express **23**, 21012 (2015).
6. C. V. Poulton, A. Yaccobi, Z. Su, M. J. Byrd, and M. R. Watts, *Advanced Photonics 2016 (IPR, NOMA, Sensors, Networks, SPPCom, SOF)* (2016), paper IW1B.2.
7. T. Komljenovic, R. Helkey, L. Coldren, and J. E. Bowers, Opt. Express **25**, 2511 (2017).
8. B. Guan, R. P. Scott, C. Qin, N. K. Fontaine, T. Su, C. Ferrari, M. Cappuzzo, F. Klemens, B. Keller, M. Earnshaw, and S. J. B. Yoo, Opt. Express **22**, 145 (2014).
9. W. S. Rabinovich, P. G. Goetz, M. Pruessner, R. Mahon, M. S. Ferraro, D. Park, E. Fleet, and M. J. DePrenger, Proc. SPIE **9354**, 93540B (2015).
10. J. Sun, "Toward accurate and large-scale silicon photonics," Ph.D. thesis (Massachusetts Institute of Technology, 2013).
11. S. Yang, Y. Zhang, T. Baehr-Jones, and M. Hochberg, Opt. Express **22**, 30607 (2014).
12. W. D. Sacher, Y. Huang, L. Ding, B. J. F. Taylor, H. Jayatilleka, G.-Q. Lo, and J. K. S. Poon, Opt. Express **22**, 10938 (2014).
13. J. Notaros, F. Pavanello, M. T. Wade, C. Gentry, A. Atabaki, L. Alloatti, R. J. Ram, and M. Popovic, *Optical Fiber Communication Conference* (2016), paper M2I.5.
14. D. Vermeulen, S. Selvaraja, P. Verheyen, G. Lepage, W. Bogaerts, P. Absil, D. V. Thourhout, and G. Roelkens, Opt. Express **18**, 18278 (2010).
15. A. Yaacobi, J. Sun, M. Moresco, G. Leake, D. Coolbaugh, and M. R. Watts, Opt. Lett. **39**, 4575 (2014).
16. D. D. John, M. J. R. Heck, J. F. Bauters, R. Moreira, J. S. Barton, J. E. Bowers, and D. J. Blumenthal, IEEE Photon. Technol. Lett. **24**, 876 (2012).
17. W. D. Sacher, Z. Yong, J. C. Mikkelsen, A. Bois, Y. Yang, J. C. Mak, P. Dumais, D. Goodwill, C. Ma, J. Jeong, E. Bernier, and J. K. Poon, *Conference on Lasers and Electro-Optics (CLEO)* (2016), paper JTh4C.3.
18. Y. Zhang, A. Hosseini, J. Ahn, D. N. Kwong, B. Fallahazad, E. Tutuc, and R. T. Chen, *IEEE Optical Interconnects Conference* (2012), pp. 54–55.
19. M. Fan, M. A. Popovic, and F. X. Kartner, *Conference on Lasers and Electro-Optics (CLEO)* (2007), pp. 1–2.